Dalton Transactions

Elucidating the Origins of Enhanced CO_2 Reduction in Manganese Electrocatalysts Bearing Pendant Hydrogen-Bond Donors

Journal:	*Dalton Transactions*
Manuscript ID	DT-ART-05-2019-002060.R1
Article Type:	Paper
Date Submitted by the Author:	08-Jul-2019
Complete List of Authors:	Tignor, Steven; Princeton University, Chemistry Shaw, Travis; Princeton University, Chemistry Bocarsly, Andrew; Princeton University, Chemistry

ARTICLE

Elucidating the Origins of Enhanced CO_2 Reduction in Manganese Electrocatalysts Bearing Pendant Hydrogen-Bond Donors

Received 00th January 20xx,
Accepted 00th January 20xx

DOI: 10.1039/x0xx00000x

Steven E. Tignor,[a] Travis W. Shaw [b] and Andrew B. Bocarsly *[a]

Complexes of the general form [Mn(X)(CO)$_3$bpy] (X = a variety of monodentate ligands, bpy = 2,2' bipyridine) have been reported to act as electrocatalysts for the reduction of CO_2 to CO. In this work, a series of phenol and anisole substituted bipyridine ligands were synthesized and ligated to a manganese metal center in order to probe for an intramolecular hydrogen-bonding interaction in the transition state of CO_2 reduction. Ligands without the ability to intramolecularly hydrogen bond displayed decreased catalytic current density compared to those with the ability to hydrogen bond with CO_2. Electrocatalysis was studied by performing voltammetric and bulk electrolysis experiments under argon or CO_2 environments. Measurements of catalytic rates using hydrogen vs. deuterium for the intramolecular H/D-bonding step show that there is an isotope effect associated with the catalysis. The data presented herein suggest a mechanism involving two subsequent equilibrium isotope effects in combination with a primary kinetic isotope effect.

Introduction

Carbon dioxide is an increasingly Earth abundant chemical which has the potential to be used as a feedstock for chemicals and fuels.[1,2] The catalytic reduction of CO_2 has been known for several decades, however it has attracted growing interest in recent years.[3,4] Electrochemical methods are uniquely suited for the catalytic reduction of CO_2 due to the high atom economy associated with these processes.[5] Among these methods, transition-metal mediated electrochemical reduction offers the ability to specifically tailor the catalytic active site to better understand the mechanism of CO_2 reduction.[6–10]

One particular type of homogenous transition-metal CO_2 reduction catalyst that is of recent interest is [MnX(CO)$_3$(bpy)], where X = Cl^-, Br^- or CN^- and bpy = 2,2'-bipyridine.[11–14] This system has shown the ability to convert CO_2 to CO with high efficiency and excellent selectivity.[15] In addition, this system has advances over the analogous rhenium system in areas such as efficiency and cost. Several groups including ours have examined variations at bpy, such as changing the ligand environment using bulky bipyridine ligands to inhibit dimerization of the catalytically active species[16] or N-heterocyclic carbene (NHC) ligands to modulate the electronics of the complex.[17–20]

Recently, there have been several reports utilizing a secondary-coordination sphere activation mode for enhanced catalysis.[21–24] In 2015, our group reported a manganese electrocatalyst containing a bipyridine ligand with a phenol moiety covalently attached to the 6-position on the bpy which demonstrated enhanced catalytic activity.[25] The performance of this new complex was markedly improved, generating 10.5 times the catalytic current of the parent complex, [MnBr(CO)$_3$bpy]. We suggested that the observed current enhancement might be attributed to intramolecular hydrogen bonding interactions at the CO_2 binding site that are generated by the pendant phenol moiety.

Herein, we present a mechanistic study supporting the viability of this proposal. We show that the catalytic enhancement is highly dependent upon the location of the phenol moiety on the bipyridine ligand, and support the intramolecular hydrogen bonding theory by gathering x-ray data to show that the hydrogen to CO_2 distances for the catalytically less active species are beyond the distance of a strong hydrogen bond. Furthermore, complexes without the ability to intramolecularly hydrogen bond (ϕ-OMe instead of ϕ-OH) displayed significant catalytic current decrease when compared to the hydrogen bonding analogues. Finally, an H/D isotope effect study is undertaken to further probe the dynamic role of an intramolecular hydrogen bond in the reduction of CO_2 to CO at a "Mn(CO)$_3$bpy" reaction center.

Results and Discussion

The hydrogen-bonding effect was studied by synthesizing a variety of substituted bipyridine ligands with phenol and anisole at the 4-, 5-, and 6-positions. The product complexes were characterized both spectroscopically (^{1}H NMR, ^{13}C NMR and FTIR) and by single crystal x-ray diffraction. See Figure 1 and Table 1 for the phenolic structural features.

The crystal structures show that the dihedral angle between the phenol and bipyridine ring is influenced by the phenol's

[a] Department of Chemistry, Princeton University, Princeton, New Jersey 08544, United States.
[b] Address here.
[c] Address here.
† Footnotes relating to the title and/or authors should appear here.
Electronic Supplementary Information (ESI) available: [details of any supplementary information available should be included here]. See DOI: 10.1039/x0xx00000x

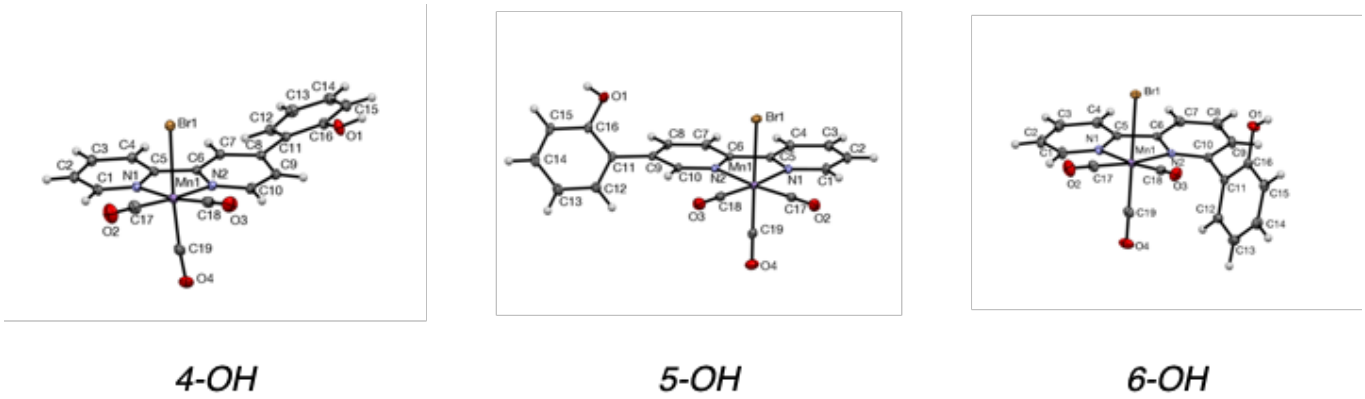

Figure 1. X-ray crystal structures of 4-OH, 5-OH, and 6-OH with ellipsoids set to 50% probability.

position around the ring. In 4-OH this dihedral angle is 24.31° and this increases to 43.40° in 5-OH followed by 64.54° in 6-OH. The increasing dihedral angle across the complexes is likely due to steric repulsion between the pendant phenol group and an equatorial CO ligand. Another indication of this steric repulsion is the Mn-N_2 (N_2 being the nitrogen contained within the pyridine ring bearing the substituent phenol) bond length data obtained from the X-ray crystal structures of the three complexes, which shows that this bond length is greatest for 6-OH (Table 1). There is very little variation in the bond length of the Mn-N_1 bond associated with the unsubstituted bipyridine ring.

Table 1. Dihedral angles, selected bond lengths, and interatomic distances for 4-OH, 5-OH, and 6-OH.

Compound	Dihedral Angle (°)	Mn-N_1 (Å)	Mn-N_2 (Å)	O-Br Interatomic Distance (Å)
4-OH	**24.31**	**2.041**	**2.028**	**6.754**
5-OH	**43.30**	**2.050**	**2.048**	**6.696**
6-OH	**64.54**	**2.035**	**2.091**	**4.425**

N1 and N2 are shown in the x-ray structures in Figure 1.

The proposed mechanism by which these Mn(I) catalysts are thought to catalyze the reduction of CO_2 to CO is given in Figure 2.[26] The primary reduction event is generally accepted to involve addition of an electron to the bpy π^* orbital. This then induces the loss of the axial bromide ligand, opening up a coordination site. A subsequent one electron reduction delivers the active catalyst, which is primed for CO_2 binding. The introduction of a carboxylate ligand is followed by two protonation steps and the loss of a molecule of water. A final electron transfer brings the catalyst back to its active state and yields a molecule of free CO as the reduced product.

The increased dihedral angle for 6-OH compared to 4- and 5-OH is convenient because this places the phenolic OH at a distance from the metal center that is more likely to allow hydrogen bonding to either a bound CO_2 or to stabilize the transition state for CO_2 bonding to the metal. In order to further explore the idea that 6-OH can enable a hydrogen bonding interaction by virtue of the distance between the phenolic oxygen to the manganese center while the other isomers cannot, we established the distance between the phenolic oxygen atom and the axial bromide using X-ray crystal structure data (see Figure 3, for example). It is important to note here that we used the bromide precursor as a proxy for the metal-carboxylate species of interest because this adduct is not sufficiently stable to be structurally characterized. This is not surprising given its assignment as a key catalytic intermediate.

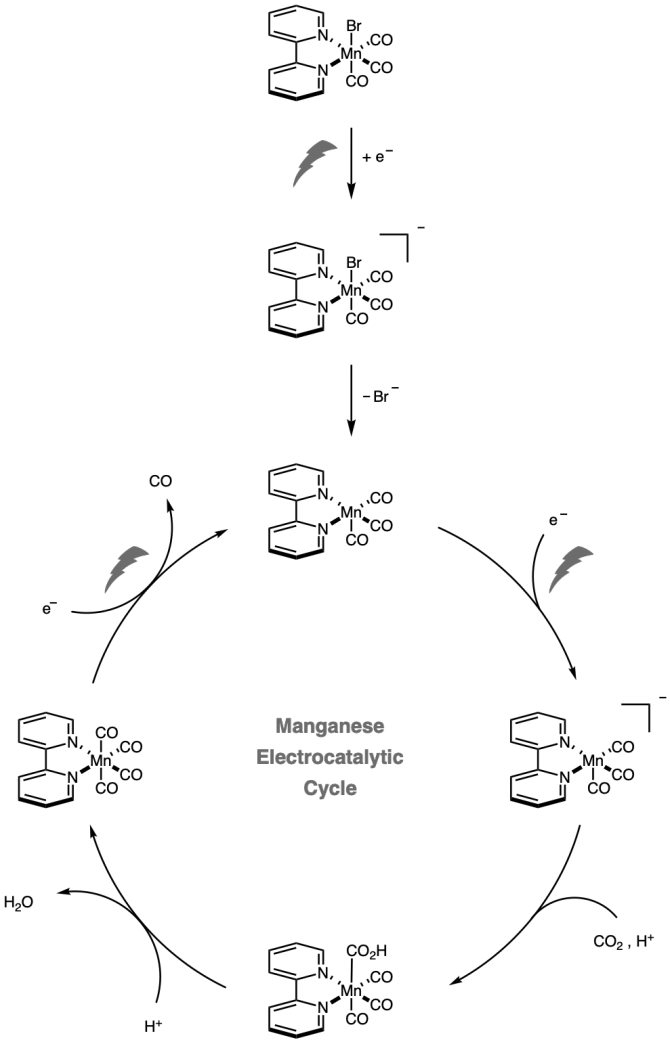

Figure 2. Electrocatalytic cycle for CO_2 reduction mediated by [Mn(bpy)$(CO)_3$Br].

We assume that the phenolic oxygen-bromide interatomic distance will accurately reflect the distance between the phenolic oxygen atom and the carbon atom of a manganese bound CO_2 complex. Under this assumption, the required distance for the hydrogen bond between the phenolic proton and the CO_2 will be approximately equal to the distance between oxygen and bromine minus an average O-H and C_{sp2}-H bond length (0.96 Å and 1.2 Å respectively[27]) as shown in Figure 3. This value corresponds to 2.3 Å for the hydrogen bond in the 6-OH, 4.5 Å for the hydrogen bond in the 5-OH, and 4.6 Å for the hydrogen bond in the 4-OH. Hydrogen bonds with distances between 2.4 Å and 2.5 Å fall into the regime of *short-strong hydrogen bonds* as categorized by Anslyn and Dougherty, meaning that the barrier for the transfer of the hydrogen atom between donor and acceptor approaches zero.[28] Furthermore, the strength of gas phase hydrogen bonds at a distance of 2.35 Å is between 30-35 kcal/mol, whereas gas phase hydrogen bonding at a distance of 3.0 Å is only stabilized by ~5 kcal/mol.[29] This rationale suggests that hydrogen-bonding interactions should be more prevalent in 6-OH than in either of the other two isomers.

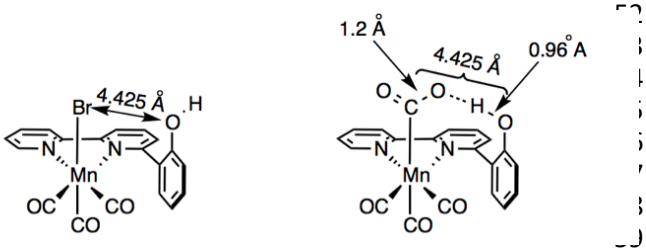

Figure 3. Interatomic distances measured from X-ray crystal structure (left). Estimation of distance required for hydrogen bond.

Additional evidence for the existence of a solution phase steric interaction is found in the ^1H and ^{13}C NMR spectra of the 6-OH complex. As shown in Figure S4, two sets of peaks indicate that there are two rotameric structures in solution: The phenolic proton exists on either the side of the complex containing the axial bromide ligand, or the side with the axial CO ligand; these two structures do not interconvert on the NMR time scale at 300 K. The 4-OH and 5-OH complexes do not display any such rotameric peaks in their NMR spectra (Figures S10 and S16).

The reduction peak potentials observed by cyclic voltammetry (CV) for the first and second electron reductions are tabulated in Table 2 for the six complexes explored (scan rate data for all complexes and conditions explored are available in Figures S19-S36). The cyclic voltammetry of 4-OH and 5-OH under argon in MeCN with 5% H_2O each show two reduction peaks at similar potentials (figures S23 and S30; for the CV of 6-OH under the corresponding conditions, see Figure S35).

Table 2. 1st and 2nd peak potentials of compounds utilized in this study.

Compound	1st Reduction Potential (V vs. SCE)	2nd Reduction Potential (V vs. SCE)
4-OH	**-1.15**	**-1.46**
4-OMe	**-1.11**	**-1.43**
5-OH	**-1.14**	**-1.44**
5-OMe	**-1.10**	**-1.40**
6-OH	**-1.14**	**-1.30**
6-OMe	**-1.21**	**-1.30**

Potentials were measured vs. Ag/Ag^+ (0.1 M in MeCN) and were subsequently converted to vs. SCE.

Overall, the CVs of 4-OH and 5-OH are very similar except for the presence of a small shoulder wave, cathodic to the second reduction wave of 5-OH (see Figure 4). The first-reduction waves for all three phenolic regioisomers are within 10 mV of each other, and the second waves are ~20 mV apart for 4-OH and 5-OH.

The second reduction waves for 6-OH and 6-OMe are shifted 140 and 100 mV anodic from 5-OH and 5-OMe, respectively. This could be due to a lack of conjugation between the phenol ring and the bipyridine ring due to a larger dihedral angle between the two rings in 6-OH and 6-OMe, as discussed previously. This would make the phenolic ring a weaker donor in this case, resulting in an anodic shift to the second wave relative to the other, better conjugated, isomers. Ultimately however, changing the connectivity to the bipyridine ring has a minimal effect on the electrochemistry under argon in MeCN with 5% H_2O.

The effect of CO_2 on the electrochemistry of 4-OH and 5-OH is much less extreme than for the case of 6-OH (Figure 4). The

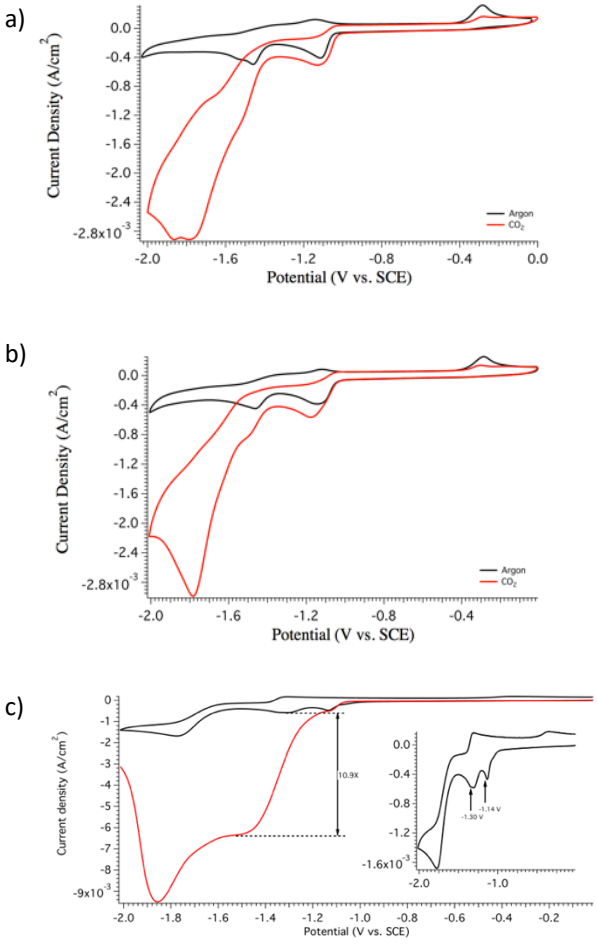

Figure 4. CVs of (a) 4-OH, (b) 5-OH, and (c) 6-OH in MeCN with 5% H_2O under argon (black) and CO_2 (red) at a scan rate of 100 mV/s.

enhancement at the second reduction wave is only ~2X for these two isomers compared to over 10X for 6-OH at 100 mV/s. In addition, this enhancement is at a greater overpotential than with the 6-OH (~500 mV overpotential compared to 400 mV for 6-OH) causing the catalytic current wave to begin overlapping with the third reduction wave. This third reduction wave, which occurs at approximately -1.8 V vs. SCE for all complexes is only present under a CO_2 atmosphere when protons are included in the electrolyte. In controlled potential electrolysis experiments of 6-OH performed in the region of this wave, visible electrode fouling was observed, leading us to associate this wave with complex decomposition. One possibility is that this wave corresponds to the reductive decomposition of the manganese carboxylate intermediate.

To determine if the phenolic moiety has a role to play outside of the proposed hydrogen bonding interaction in the 4-OH or 5-OH complexes, we also studied the voltammetry of the methylated complexes, 4-OMe and 5-OMe. Methylation has a very minimal effect on the reduction potentials and overall shape of the voltammograms for both complexes under argon as shown in Table 2 and Figure 5. In MeCN with 5% H_2O under CO_2, both complexes show a very similar current enhancement to that of their unmethylated analogs, both increasing by 1.25X (Figure 4). Based on the observation that the methylated analogs are essentially just as active for CO_2 reduction as the phenolic systems, we conclude that the phenolic proton plays an insignificant role in the behavior of 4-OH and 5-OH complexes. Notably, this rules out a local proton concentration effect due to the similarities between the –OMe and –OH species of the 4- and 5-substituted complexes.

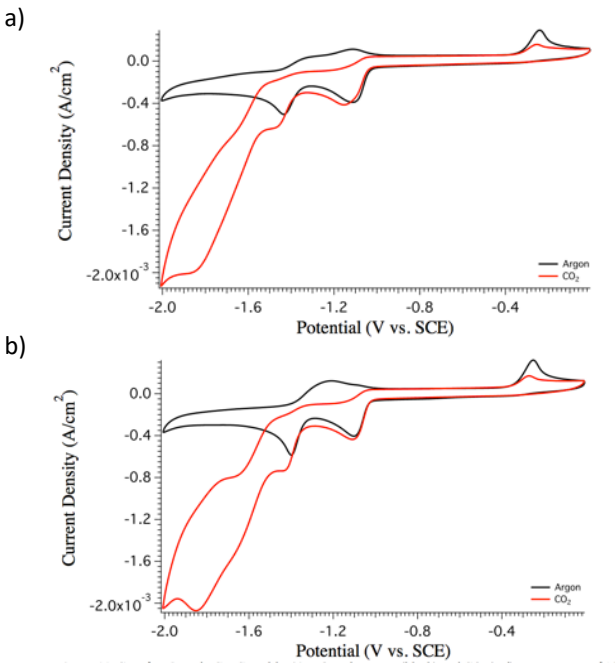

Figure 5. CVs of (a) 4-OMe and (b) 5-OMe with 5% H_2O under argon (black) and CO_2 (red) at a scan rate of 100 mV/s.

Given that a phenol placed at the 6-position enhances catalytic performance compared to a phenol incorporated at the 5- or 4-position, we sought to better understand the mechanistic underpinnings of this effect. Trivially, protons are required for catalytic conversion of CO_2 to CO; these protons may be for the CO_2 bonding step, or for the C-O bond-breaking step, or for both. The phenolic proton could be enabling CO_2 binding the metal center by forming a hydrogen bond to an incoming CO_2 molecule. This proton-assisted binding would aid in the process of rehybridization, which is one of the barriers in the conversion of CO_2 to CO. Additionally, since the overall chemical process of CO_2 conversion to CO requires two protons and two electrons (forming water in addition to CO), the phenolic proton could be acting as a simple proton donor to facilitate the conversion. To determine if the phenolic moiety could enable C-O bond cleavage, we performed CVs of the complexes in dry MeCN under a CO_2 atmosphere and looked for catalytic current enhancement (Figures 6).

The cyclic voltammetry of 4-OH and 5-OH show no signs of

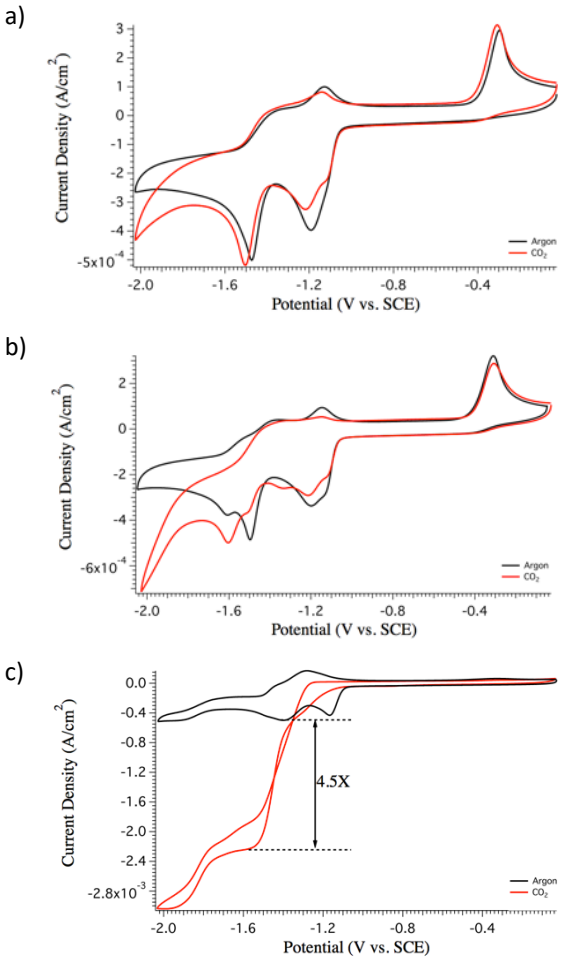

Figure 6. CVs of (a) 4-OH, (b) 5-OH, and (c) 6-OH in dry MeCN under argon (black) and CO2 (red) at a scan rate of 100 mV/s.

catalysis under anhydrous CO_2 (Figure 6a and 6b). The peak shapes for 5-OH are altered in the presence of CO_2, but no current enhancement can be detected. This may indicate that CO_2 binds to the metal center but no subsequent catalysis occurs. This could signify that the phenol moiety of 5-OH is capable of favoring CO_2 binding, but is not capable of facilitating subsequent catalysis. Voltammetry of the 6-OH isomer is

drastically different under CO_2 than it is under argon in dry MeCN, as it displays a catalytic current enhancement of 4.5x with an onset at the second reduction wave (Figure 6c) and a plateau density, which is indicative of an electrocatalytic process.

It is possible that in 6-OH the phenol facilitates bonding of CO_2 via an intramolecular hydrogen bond, and once bound, the phenolic proton can intermolecularly aid in catalytic turnover. We reason that if appending the phenol at the 6-position aids in CO_2 binding *only*, we would see a large effect from adding free phenol when the CV was performed on 6-OH in dry MeCN under a CO_2 atmosphere. If the phenolic moiety helps facilitate C-O bond breaking via a transition state that is dependent on the proximity and geometry of the phenol relative to the CO_2 ligand, then adding phenol to the electrolyte should have little effect.

Figure 7 shows the effect of adding 1, 2, and 10 mM phenol to a cell containing 1 mM 6-OH in dry MeCN under CO_2. No significant current enhancement over the complex alone is observed, even when the proton concentration of the solution is increased by an order of magnitude. This result suggests that the unique position of the phenolic moiety aids in binding and is also important in C-O bond cleavage via an intramolecular pathway.

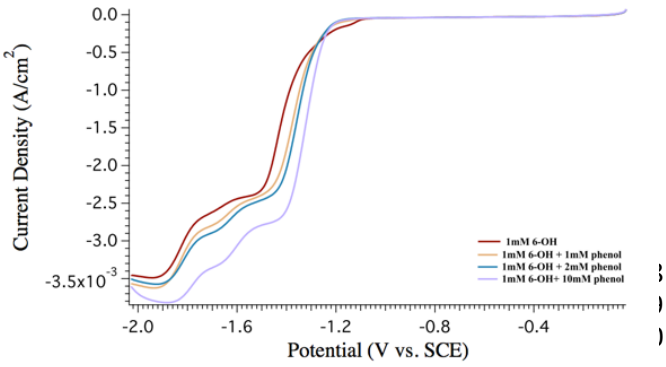

Figure 7. Linear sweep voltammetry of 6-OH in dry MeCN under CO_2 with varying amounts of phenol added to the electrolyte.

The hydrogen-bonding effect associated with the 6-OH complex should be eliminated under wet electrolyte when the 6-OMe complex is used instead. This is what is observed experimentally: the 6-OMe complex displays a significant loss in current enhancement by CV when compared to the 6-OH complex (Figures S37-S38). Importantly, the 6-OMe complex does display superior current enhancement compared to the parent complex, indicating the location of the substituent is facilitating catalysis, albeit not through an intramolecular hydrogen bond. This result is in agreement with Ngo *et. al.* and highlights the importance of Lewis basic moieties in close proximity to the open coordination site, thereby switching on what they have referred to as a 'protonation-first' pathway.[24]

Isotope Effect Studies

To further elucidate the mechanism of catalytic turnover, a series of isotope effect experiments were conducted on the parent complex as well as the 4-OH and the 6-OH complexes. Experiments using 5% H_2O and 95% MeCN (v/v) were performed on both complexes, as well as experiments using 5% D_2O and 95% MeCN. The acidity of phenol assures rapid exchange of the phenol proton with H_2O (or D_2O) in the mixed solvent systems employed. In the presence of 5% D_2O, there is almost exclusively deutrophenol present when 1mM of Mn-complex is introduced, and thus, this system provides an environment for probing the H/D isotope kinetics exclusively at the phenolic site.

To test the viability of using the described solvent system to probe for an H/D isotope effect a series of cyclic voltammograms using the 6-OH complex were collected under a CO_2 atmosphere with either 5% H_2O or 5% D_2O in the electrolyte. Recall that the observed current is a direct measure of the rate of reaction for any reaction sequence that involves one or more charge transfer steps. As shown in Figure 8, there

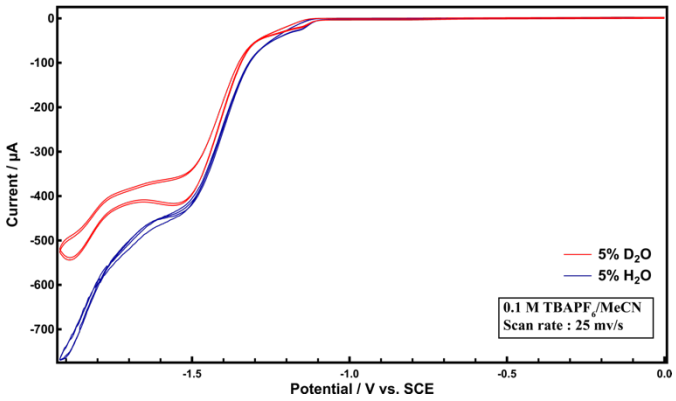

Figure 8. Cyclic voltammetry of the 6-OH complex in either 5% H_2O/95% MeCN (blue trace) or 5% D_2O/95% MeCN.

is a current enhancement using 5% H_2O versus 5% D_2O for the 6-OH complex, consistent with an isotope effect. This isotope effect was quantified by doing bulk electrolysis experiments, which gave a direct measurement of the rate of reaction by analyzing CO formation over time. The existence of a rate limiting step during the binding of CO_2 to the metal center would be expected to produce a primary KIE due to the need to break the phenolic O-H bond.

Bulk electrolysis experiments were conducted just past the second CV reduction wave, at -1.72 V vs. SCE using the 5% H_2O or 5% D_2O conditions with the parent complex, the 4-OH, and the 6-OH complexes. Samples of the headspace were taken every 20 minutes for 3 hours. The slope of the line of best fit of these time points is a direct measurement of the rate of CO_2 reduction and thus, the ratio of the slopes for a complex under

Table 3. Slope of line of best fit for each plot and corresponding isotope effect.

Compound	Condition	Slope (μmol CO/min.)	F.E. (%)	Overall Isotope Effect
Parent	5% H_2O	1.37	76.4	1.05
Parent	5% D_2O	1.34	53.2	
4-OH	5% H_2O	1.89	57.3	1.37
4-OH	5% D_2O	1.55	54.6	
6-OH	5% H_2O	2.67	77.6	1.61
6-OH	5% D_2O	1.90	43.8	

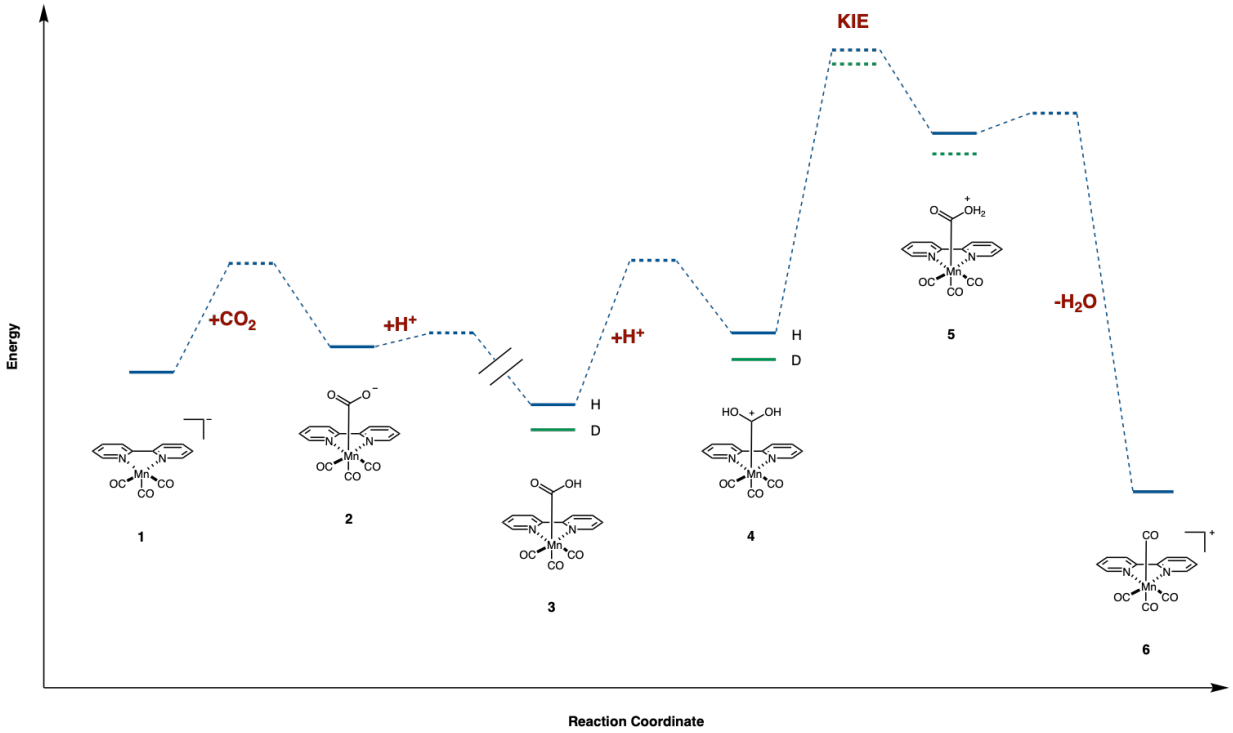

Figure 9. A proposed reaction coordinate diagram which takes into account two equilibrium isotope effects as well as a kinetic isotope effect. [$\Delta G_{1\rightarrow2}$ = +2.2 kcal/mol; $\Delta G^{\ddagger}_{1\rightarrow2}$ = +3.3 kcal/mol; $\Delta G_{2\rightarrow3}$ = -33.4 kcal/mol; $\Delta G^{\ddagger}_{2\rightarrow3}$ = barrierless; $\Delta G_{3\rightarrow6}$ = -27.8 kcal/mol; $\Delta G^{\ddagger}_{3\rightarrow6}$ = +11.9 kcal/mol; these values are based on calculations and are from Riplinger *et. al.*][26]

either the 5% H_2O or 5% D_2O conditions is a quantitative measure of the overall H/D isotope effect. The CO production rates, Faradaic efficiencies, and current vs. time plots are provided in Figures S39-S40 and summarized in Table 3 and clearly support the involvement of the phenolic proton due to the increase in the measured isotope effect from the parent complex to the 4-OH to the 6-OH. Figure 7, which reports the phenol-free control demonstrates that there is a minimal dependence on the extraneous proton source in solution. Thus, the difference in rates of CO production as shown in Figure S39 and Table 3 must be coming from the difference between a phenolic –OH vs. a phenolic –OD. Furthermore, as the location of the pendant phenolic position becomes more ideal for binding to an incoming CO_2, the magnitude of the isotope effect increases accordingly, suggesting this position is crucial for the catalytic rate of these complexes.

There is a clear trend in the isotope effect data in which the greater the ability the complex has to intramolecularly hydrogen bond, the greater the value of the observed overall isotope effect. These data experimentally confirm the prior computational work done by our group as well as that of Carter and Kubiak, where it was proposed that proton-assisted C-O bond cleavage is the rate limiting step. However, pre-equilibria prior to the rate limiting step occur, each affecting the overall rate through an equilibrium isotope effect. Here, the measured overall isotope effect is an amalgamation of these equilibrium isotope effects and a kinetic isotope effect for the C-O bond cleavage event. The magnitude of the overall isotope effect is largest for phenolic moieties positioned optimally for intramolecular hydrogen bonding, and the magnitude decreases according to the strength of the intramolecular interaction. Based on the results presented by Carter and Kubiak[26], we propose a mechanism for this overall isotope effect measurement, which is shown in Figure 9. This reaction coordinate diagram utilizes the previous calculation data from Carter and Kubiak to generate the reaction coordinate profile for intermediates **1**, **2**, **3**, and **6**. Intermediates 4 and 5 represent likely intermediates in going from complex 3 to complex 6. Notably, this reaction coordinate scheme takes into account the equilibrium isotope effects and subsequent kinetic isotope effect that are in agreement with our experimental rate data.

Conclusions

A series of 2-hydroxyphenyl- and 2-methoxyphenyl-substituted bipyridine ligands were synthesized in order to understand how hydrogen-bond donors in the second coordination sphere affect electrocatalytic CO_2 reduction using a manganese-based electrocatalyst. Voltammetric studies were performed in order to assess the reactivity of the complexes. We observed that significant catalytic current enhancement beyond the unsubstituted bipyridine complex was only realized when the pendant phenol was placed at the 6-position of the bipyridine ligand, the position closest to the ligated metal center. Not only is the phenolic proton's distance minimized when the phenol is at the 6-position, but the torsion angle between the phenol ring and the bipyridine ring may be increased relative to 4- and 5-substituted complexes due to steric interference between the phenol and the manganese center as indicated by X-ray crystal

structures of the complex. The result is a phenolic proton positioned to facilitate binding of a CO_2 ligand and a C-O bond-breaking event of a bound CO_2 ligand. A series of H/D isotope effect experiments were performed to gain further mechanistic insight. From the data collected there was a clear trend in the value of the observed isotope effect, which correlates well with the complex's ability to intramolecularly hydrogen bond affecting both the hypothesized reactive intermediates and the transition state associated with cleavage of the carbon dioxide C–O bond.

Conflicts of interest

There are no conflicts to declare.

Acknowledgements

Financial support for this work was provided by the National Science Foundation under grant CHE-1800400. Any opinions, findings, and conclusions or recommendations expressed in this material are those of the authors and do not necessarily reflect the views of the National Science Foundation.

Notes and references

(1) Whipple, D. T.; Kenis, P. J. A. Prospects of CO2 Utilization via Direct Heterogeneous Electrochemical Reduction. *J. Phys. Chem. Lett.* **2010**, *1* (24), 3451–3458. https://doi.org/10.1021/jz1012627.

(2) Rafiee, A.; Rajab Khalilpour, K.; Milani, D.; Panahi, M. Trends in CO_2 Conversion and Utilization: A Review from Process Systems Perspective. *J. Environ. Chem. Eng.* **2018**, *6* (5), 5771–5794. https://doi.org/10.1016/j.jece.2018.08.065.

(3) Wang, W.-H.; Himeda, Y.; Muckerman, J. T.; Manbeck, G. F.; Fujita, E. CO_2 Hydrogenation to Formate and Methanol as an Alternative to Photo- and Electrochemical CO_2 Reduction. *Chem. Rev.* **2015**, *115* (23), 12936–12973. https://doi.org/10.1021/acs.chemrev.5b00197.

(4) Jones, J.-P.; Prakash, G. K. S.; Olah, G. A. Electrochemical CO2 Reduction: Recent Advances and Current Trends. *Isr. J. Chem.* **2014**, *54* (10), 1451–1466. https://doi.org/10.1002/ijch.201400081.

(5) Bushuyev, O. S.; De Luna, P.; Dinh, C. T.; Tao, L.; Saur, G.; van de Lagemaat, J.; Kelley, S. O.; Sargent, E. H. What Should We Make with CO_2 and How Can We Make It? *Joule* **2018**, *2* (5), 825–832. https://doi.org/10.1016/j.joule.2017.09.003.

(6) Kumagai, H.; Nishikawa, T.; Koizumi, H.; Yatsu, T.; Sahara, G.; Yamazaki, Y.; Tamaki, Y.; Ishitani, O. Electrocatalytic Reduction of Low Concentration CO_2. *Chem. Sci.* **2019**, *10* (6), 1597–1606. https://doi.org/10.1039/C8SC04124E.

(7) Kaminsky, C. J.; Wright, J.; Surendranath, Y. Graphite-Conjugation Enhances Porphyrin Electrocatalysis. *ACS Catal.* **2019**, 3667–3671. https://doi.org/10.1021/acscatal.9b00404.

(8) Sampson, M. D.; Kubiak, C. P. Manganese Electrocatalysts with Bulky Bipyridine Ligands: Utilizing Lewis Acids To Promote Carbon Dioxide Reduction at Low Overpotentials. *J. Am. Chem. Soc.* **2016**, *138* (4), 1386–1393. https://doi.org/10.1021/jacs.5b12215.

(9) Takeda, H.; Ohashi, K.; Sekine, A.; Ishitani, O. Photocatalytic CO_2 Reduction Using Cu(I) Photosensitizers with a Fe(II) Catalyst. *J. Am. Chem. Soc.* **2016**, *138* (13), 4354–4357. https://doi.org/10.1021/jacs.6b01970.

(10) Froehlich, J. D.; Kubiak, C. P. The Homogeneous Reduction of CO_2 by $[Ni(Cyclam)]^+$: Increased Catalytic Rates with the Addition of a CO Scavenger. *J. Am. Chem. Soc.* **2015**, *137* (10), 3565–3573. https://doi.org/10.1021/ja512575v.

(11) Machan, C. W.; Stanton, C. J.; Vandezande, J. E.; Majetich, G. F.; Schaefer, H. F.; Kubiak, C. P.; Agarwal, J. Electrocatalytic Reduction of Carbon Dioxide by Mn(CN)(2,2'-Bipyridine)$(CO)_3$: CN Coordination Alters Mechanism. *Inorg. Chem.* **2015**, *54* (17), 8849–8856. https://doi.org/10.1021/acs.inorgchem.5b01715.

(12) Agarwal, J.; Iii, C. J. S.; Shaw, T. W.; Vandezande, J. E.; Majetich, G. F.; Bocarsly, A. B.; Iii, H. F. S. Exploring the Effect of Axial Ligand Substitution (X = Br, NCS, CN) on the Photodecomposition and Electrochemical Activity of $[MnX(N–C)(CO)_3]$ Complexes. *Dalton Trans.* **2015**, *44* (5), 2122–2131. https://doi.org/10.1039/C4DT03079F.

(13) Bourrez, M.; Molton, F.; Chardon-Noblat, S.; Deronzier, A. $[Mn(Bipyridyl)(CO)_3Br]$: An Abundant Metal Carbonyl Complex as Efficient Electrocatalyst for CO_2 Reduction. *Angew. Chem. Int. Ed.* **2011**, *50* (42), 9903–9906. https://doi.org/10.1002/anie.201103616.

(14) Grills, D. C.; Ertem, M. Z.; McKinnon, M.; Ngo, K. T.; Rochford, J. Mechanistic Aspects of CO_2 Reduction Catalysis with Manganese-Based Molecular Catalysts. *Coord. Chem. Rev.* **2018**, *374*, 173–217. https://doi.org/10.1016/j.ccr.2018.05.022.

(15) Smieja, J. M.; Sampson, M. D.; Grice, K. A.; Benson, E. E.; Froehlich, J. D.; Kubiak, C. P. Manganese as a Substitute for Rhenium in CO_2 Reduction Catalysts: The Importance of Acids. *Inorg. Chem.* **2013**, *52* (5), 2484–2491. https://doi.org/10.1021/ic302391u.

(17) Franco, F.; Pinto, M. F.; Royo, B.; Lloret-Fillol, J. A Highly Active N-Heterocyclic Carbene Manganese(I) Complex for Selective Electrocatalytic CO_2 Reduction to CO. *Angew. Chem. Int. Ed.* **2018**, *57* (17), 4603–4606. https://doi.org/10.1002/anie.201800705.

(18) Myren, T. H. T.; Lilio, A. M.; Huntzinger, C. G.; Horstman, J. W.; Stinson, T. A.; Donadt, T. B.; Moore, C.; Lama, B.; Funke, H. H.; Luca, O. R. Manganese N-Heterocyclic Carbene Pincers for the Electrocatalytic Reduction of Carbon Dioxide. *Organometallics* **2019**, *38* (6), 1248–1253. https://doi.org/10.1021/acs.organomet.8b00535.

(19) Stanton, C. J.; Vandezande, J. E.; Majetich, G. F.; Schaefer, H. F.; Agarwal, J. Mn-NHC Electrocatalysts: Increasing π Acidity Lowers the Reduction Potential and Increases the Turnover Frequency for CO_2 Reduction. *Inorg. Chem.* **2016**, *55* (19), 9509–9512. https://doi.org/10.1021/acs.inorgchem.6b01657.

(20) Agarwal, J.; Shaw, T. W.; Stanton, C. J.; Majetich, G. F.; Bocarsly, A. B.; Schaefer, H. F. NHC-Containing Manganese(I) Electrocatalysts for the Two-Electron Reduction of CO_2. *Angew. Chem. Int. Ed.* **2014**, *53* (20), 5152–5155. https://doi.org/10.1002/anie.201311099.

(21) Costentin, C.; Drouet, S.; Robert, M.; Savéant, J.-M. A Local Proton Source Enhances CO_2 Electroreduction to CO by a

Molecular Fe Catalyst. *Science* **2012**, *338* (6103), 90–94. https://doi.org/10.1126/science.1224581.

(22) Franco, F.; Cometto, C.; Nencini, L.; Barolo, C.; Sordello, F.; Minero, C.; Fiedler, J.; Robert, M.; Gobetto, R.; Nervi, C. Local Proton Source in Electrocatalytic CO_2 Reduction with [Mn(Bpy–R)$(CO)_3$Br] Complexes. *Chem. – Eur. J.* **2017**, *23* (20), 4782–4793. https://doi.org/10.1002/chem.201605546.

(23) Chapovetsky, A.; Welborn, M.; Luna, J. M.; Haiges, R.; Miller, T. F.; Marinescu, S. C. Pendant Hydrogen-Bond Donors in Cobalt Catalysts Independently Enhance CO_2 Reduction. *ACS Cent. Sci.* **2018**, *4* (3), 397–404. https://doi.org/10.1021/acscentsci.7b00607.

(24) Ngo, K. T.; McKinnon, M.; Mahanti, B.; Narayanan, R.; Grills, D. C.; Ertem, M. Z.; Rochford, J. Turning on the Protonation-First Pathway for Electrocatalytic CO_2 Reduction by Manganese Bipyridyl Tricarbonyl Complexes. *J. Am. Chem. Soc.* **2017**, *139* (7), 2604–2618. https://doi.org/10.1021/jacs.6b08776.

(25) Agarwal, J.; Shaw, T. W.; Schaefer, H. F.; Bocarsly, A. B. Design of a Catalytic Active Site for Electrochemical CO_2 Reduction with Mn(I)-Tricarbonyl Species. *Inorg. Chem.* **2015**, *54* (11), 5285–5294. https://doi.org/10.1021/acs.inorgchem.5b00233.

(26) Riplinger, C.; Sampson, M. D.; Ritzmann, A. M.; Kubiak, C. P.; Carter, E. A. Mechanistic Contrasts between Manganese and Rhenium Bipyridine Electrocatalysts for the Reduction of Carbon Dioxide. *J. Am. Chem. Soc.* **2014**, *136* (46), 16285–16298. https://doi.org/10.1021/ja508192y.

(27) Huheey, J. E. *Inorganic Chemistry Principles of Structure and Reactivity (4th Edition)Hardcover*, 4 edition.; Prentice Hall, 1997.

(28) Anslyn, E. V.; Dougherty, D. A. *Modern Physical Organic Chemistry*; University Science Books, 2006.

(29) Advances in Physical Organic Chemistry, Volume 26 - 1st Edition https://www.elsevier.com/books/advances-in-physical-organic-chemistry/bethell/978-0-12-033526-8 (accessed Apr 2, 2019).